DINCON 2017
CONFERÊNCIA BRASILEIRA DE DINÂMICA, CONTROLE E APLICAÇÕES
30 de outubro a 01 de novembro de 2017 – São José do Rio Preto/SP

ANALYSIS OF VORTEX-INDUCED VIBRATION OF VARIABLE-TENSION VERTICAL RISERS IN LINEARLY SHEARED CURRENTS

Félix Ernesto Salazar Marín[1]

Centro de Engenharia, Modelagem e Ciências Sociais, UFABC, Santo André, SP

Juan Pablo Julca Avila[2]

Centro de Engenharia, Modelagem e Ciências Sociais, UFABC, Santo André, SP

Abstract. The main aim of this work is to simulate Vortex-Induced Vibration (VIV) in top tensioned long risers deep-water using a computational tool, written in FORTRAN, developed and implemented in advanced. A top tensioned riser is modeled as a vertical Euler-Bernoulli beam. A code for the static and dynamic analysis by Finite Element Method is developed. The 3D fluid flow around the riser is replaced by a determinate number of 2D cross-sections. In each hydrodynamic cross-section, fluid flow is calculated by the Discrete Vortex Method (DVM) to obtain drag and lift forces. Dynamics equations are solved using hydrodynamic forces previously calculated to get the dynamics-time response of vertical riser. The developed computational tool was implemented in the UFABC's cluster using High-Performance Computing techniques.

Keywords. Top tensioned riser, Vortex-Induced Vibration, Finite Element Method, Discrete Vortex Method, High-Performance Computing.

1 Introduction

Risers are long, tubular and cylindrical structures used to transfer oil and gas from an oil well located on the seabed to a floating oil production platform. Immersed in currents, the risers vibrate due to the cyclic hydrodynamic forces induced by the alternating vortices in downstream. This phenomenon is known as VIV. When the frequency of vortex emission approaches one of the natural frequencies of the riser, it begins to oscillate and takes control of the vortex shedding process, and subsequently, when the frequency of vortex shedding coincides with the natural frequency of the riser, it rises to resonance. This phenomenon is called lock-in or synchronization. In lock-in, risers vibrate with large amplitudes and are subjected to high cyclic bending stress, which can lead to premature failure due to fatigue.

[1]felix.salazar@ufabc.edu.br
[2]juan.avila@ufabc.edu.br

VIV is a problem that occurs in many fields of the engineer and its importance has led to many studies which are extensively revised in [7] and [1]. However, most of these studies focus on VIV of short rigid cylinders mounted on an elastic base where the aspect ratio (ratio of length to diameter) is less than 100.

Long risers with a high aspect ratio (of the order of 1,000 units) are required to operate in ultra-deep water and understanding the VIV of these structures is more complicated than the VIV of short cylinders. The VIV of long cylinders is characterized by the following phenomena: 1) multimodal vibration 2) dynamic response equally important both in the direction of the current and transverse to this 3) lock- In non-stationary 4) importance of the third and higher modes of vibration in the dynamic response and 5) response dominated by waves propagating along the riser. The simultaneous occurrence of these phenomena makes the VIV study of ultra-deep-water risers, a highly complex problem and many numerical and experimental research should be done to understand the dynamics of these structures.

The literature review shows that the VIV of long risers with high aspect ratio tensioned at the top hasn't been fully understood, but there are discrepancies in the literature outcomes, it is still an open field research.

This work proposes the development and implementation in FORTRAN of a computational tool capable of simulating the VIV of long risers drawn at the top.

2 Purpose

This work proposes the development and implementation in FORTRAN language of a computational tool capable of simulating VIV in long risers for deep-water.

3 Mathematical Modeling

It was formulated the equations of lateral movement of a flat beam with both its articulated ends and subjected to a variable axial force. As the axially tensioned riser is seen as a slender beam with a high aspect ratio, where the shear stresses can be omitted and the cross section at any point remains flat and perpendicular to the beam axis, in this work was adopted EULER-BERNOULLI beam theory for the modeling of riser, object of study.

We also used the spatial and temporal discretization by Finite Elements of the riser equation, using the GALERKIN approach. Structural dynamics equations are presented in the standard form for their implementation.

3.1 Equations of motion of vertical riser

A Cartesian coordinate system originating from the riser base was used, the x-axis is parallel to the velocity of the marine current, the x-axis coincides with the riser axis, and the y-axis is perpendicular to both. The displacements of a point of the riser at time t and the directions x, y and z are respectively, *u(z,t)*, *v(z,t)* and *w(z,t)*.

The riser material under study has an elastic behavior and, consequently, undergoes small deformations. In addition, the riser is subjected to small displacements, so any kind of geometric nonlinearity due to large displacements is disregarded. The geometric nonlinearity is due to the misalignment of the axial forces, leading to the addition of a bending moment term in the equations of movement of the riser. Figure 1 shows the deflected configuration of the beam that models the riser.

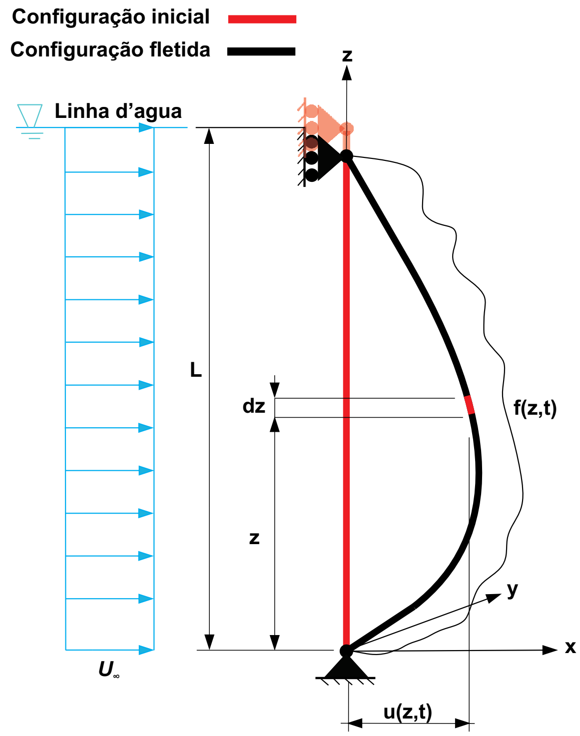

Figure 1: Reference system of the Cartesian axes.

The equation that governs the static behavior of the vertical riser (see [6]) is given by Eq. (3.1) and is presented here as:

$$\frac{\partial^2}{\partial z^2}\left[EI\frac{\partial^2 u}{\partial z^2}\right]-(T_t-y_sA_s(L-s)+p_oA_o-p_iA_i)\frac{\partial^2 u}{\partial z^2}=q+(y_sA_s-y_oA_o+y_iA_i)\frac{du}{dz} \quad (3.1)$$

where T_t is the axial force at the top of the riser and y_s is the specific gravity of the riser material in the air. p_o and p_i are the external and internal pressure respectively. A_s, A_i and A_o are the cross-sectional area of the riser wall, the cross-sectional area of the internal riser bore and the cross-sectional area of the riser respectively, and z is the position coordinate of a point on the riser axis and q is the hydrodynamic loading.

Applying GALERKIN approach and the Finite Element Method (FEM), the Eq. (3.1) is expressed in matrix form as:

$$\{[K_E]+[K_G(u)]\}=\{f(t)\} \quad (3.2)$$

where $[K_E]$ and $[K_G(u)]$ are the matrices of elastic stiffness and geometric stiffness respectively, and $f(t)$ is the vector of external forces. These last term includes the weight itself, the drag and the forces of inertia occasioned by the fluid.

To solve Eq. (3.2) it is necessary to iterate because $[K_G(u)]$ is a function of the displacement vector, as described by [4]. In case of a riser that has a slight inclination, Eq. (3.3) is valid. For a vertical riser, $\dfrac{du}{dz}$ is zero, the second term on right hand of Eq. (3.1) is neglected.

$$\frac{du}{dz} = \frac{\Delta x}{L} \tag{3.3}$$

The method used to calculate the static configuration of riser is called "Secant Stiffness" by [3]. The last iteration of this method will become the stiffness matrix $[K]$ in the equation that governs the dynamic response of the riser. This equation with various degrees of freedom is formulated as:

$$[M]\{\ddot{d}(t)\} + [C]\{\dot{d}(t)\} + [K]\{d(t)\} = \{f(t)\} \tag{3.4}$$

where $[M]$ is the mass matrix, $[C]$ is the damping matrix, $[K]$ is the stiffness matrix, $\ddot{d}(t)$, $\dot{d}(t)$ and $d(t)$ are the acceleration, velocity and displacement vectors respectively and $f(t)$ is the vector of external forces.

The difference in the static analysis developed that uses the consistent stiffness matrix, in the dynamic analysis this reduction omits the vertical degrees of freedom and rotations (hypothesis), related to the axial displacements and moments respectively. Therefore, only the horizontal degrees of freedom related to movements in the plane of the paper and in the transverse plane are considered. In the study, the reduced matrix was used because of the assumed hypothesis.

It should be noted that the consistent stiffness matrix has better accuracy when performing dynamic analysis, but this improvement is small. The obtained matrix, omitting the degrees of freedom related to axial displacements and rotations, was used because it was smaller and ensure good results without losing much precision.

The Discrete Vortex Method (MVD) using the two-dimensional sections only allows the calculation of the external forces in the x- and y-direction, so that the external axial forces can't be calculated. Because of this, the application of the reduced matrix because of the assumed hypothesis is convenient.

The problem will be approached by assembling two independent systems, related to Eq. (3.4), for dynamic analysis. The equations in the x and y directions are:

$$[M]\{\ddot{x}(t)\} + [C]\{\dot{x}(t)\} + [K]\{x(t)\} = \{f_x(t)\} \tag{3.5}$$

$$[M]\{\ddot{y}(t)\} + [C]\{\dot{y}(t)\} + [K]\{y(t)\} = \{f_y(t)\} \tag{3.6}$$

In the dynamic analysis, the matrices of Eq. (3.5) and Eq. (3.6) are invariant during the simulation. $\ddot{x}(t)$, $\dot{x}(t)$ and $x(t)$ are the vectors related to acceleration, velocity and displacement of the nodes in the x direction respectively. $\ddot{y}(t)$, $\dot{y}(t)$ and $y(t)$ are the vectors related to acceleration, velocity and displacement of the nodes, in the direction y respectively. $f_x(t)$ and $f_y(t)$ are the external forces, in the x- and y- directions respectively.

In case of the stiffness matrix in the x-axis, the Eq. (3.5), the matrix related to its deflected configuration is used. This matrix remains constant during dynamic analysis. The matrix related to an already deflected configuration is similar to a mean configuration of the structure in the study of vibrations. On the other hand, the stiffness matrix in the y-axis, the Eq. (3.6), uses the initial configuration of the riser which is the average configuration around which the vibrations occur.

3.2 Discrete Vortex Method

The wall of the body is discretized in a number of panels. On each of them a circulation vortex Γ_i located at a distance δ_0 from the panel is generated. The vortex size created is equal to the initial size σ_0 of the vortex nucleus in the center of each panel, see the detail of Figure 2.

Figure 2 shows the discretization by panels of a circular boundary. In the highlighted panel z_p indicates its coordinates. Henceforth all variables indicating position will be represented in the form of complex numbers $z = x + iy$. The position of the center of the panel is given by the complex number z_w. Similarly, z_c is the position of the created vortex and z_k represents the coordinate of a vortex already existing on the wake. Γ_i is the circulation of the generated vortex, Γ_k is the circulation of the existing vortex, and finally, U_∞ and V_∞ are the velocity components of the freestream, in the x and y axes, respectively.

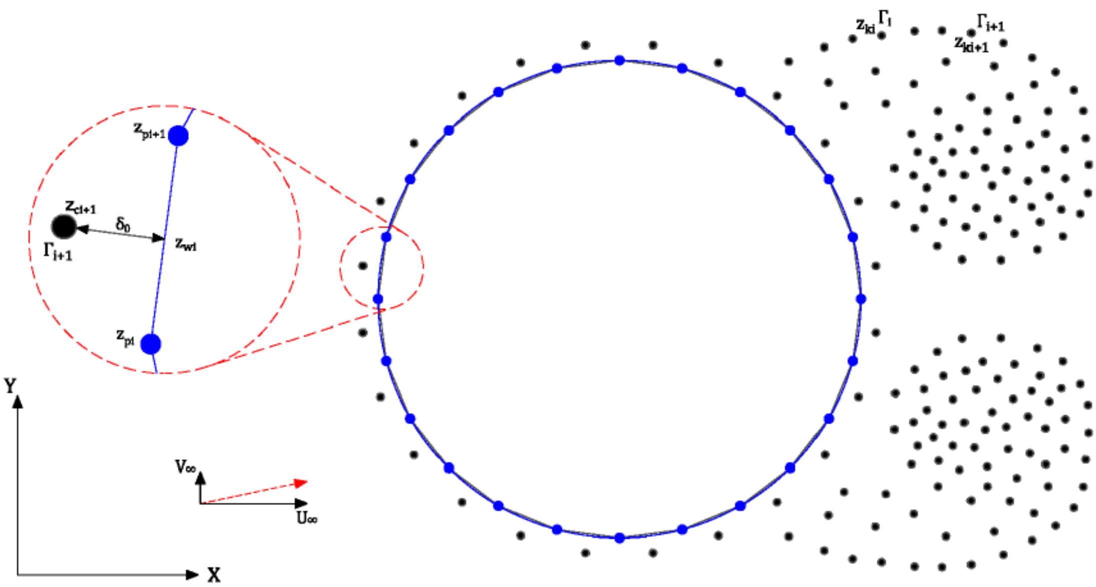

Figure 2: Discretization in panels of the body by [8].

By the principle of superposition, the stream function ψ_i in the panel (at its center) i of the body is a linear combination of three components: the free stream function, the stream function associated with the vortices created around the boundary of the body and free vortices already existing in the flow:

$$\psi_i = \mathrm{Im}\left|z_{wi}\left(U_\infty - iV_\infty\right)\right| - \frac{1}{4\pi}\sum_{i=1}^{N_w}\Gamma_i \ln\left(\left|z_{wi}-z_{cj}\right|^2+\sigma_0^2\right)$$
$$-\frac{1}{4\pi}\sum_{k=1}^{N_v}\Gamma_k \ln\left(\left|z_{wi}-z_{kj}\right|^2+\sigma^2\right) \tag{3.7}$$

for $j = 1, 2, \ldots, N_w$ and $k = 1, 2, \ldots, N_v$.

The flow must satisfy the condition of impenetrability on the wall of the body. Then, the body surface should be written as a streamline and for this the following condition should occur:

$$\psi_{i+1} - \psi_i = 0 \tag{3.8}$$

where ψ_i is the stream function on the side panel i.

The Eq. (3.8) is for a case of the stationary body, there isn't mass flow through the body. If the body were in motion, in order to guarantee the impenetrability on the wall, it is necessary that the difference between the stream functions of two consecutive points in the boundary be equal to the flow that would enter, by those same points, due to the movement of the body, therefore the Eq. (3.8) adopts the following form:

$$\psi_{i+1} - \psi_i = -\left(V_B \cdot \hat{n}\right) \cdot \Delta s \tag{3.9}$$

where V_B is the translation velocity of the body, $\hat{n}$ is the vector normal to the panel and Δs is the panel length. Substituting Eq. (3.9) into Eq. (3.7) and applying to all panels, we obtain a system of linear algebraic equations, having as unknowns the circulations Γ_j of newly created vortices:

$$[A]\{\Gamma\} = \{B\} \tag{3.10}$$

where the components of matrix $[A]$ and vector $\{B\}$ are, respectively:

$$a_{ij} = \frac{1}{4\pi}\ln\left(\frac{\left|z_{wi+1}-z_{cj}\right|^2+\sigma_0^2}{\left|z_{wi}-z_{cj}\right|^2+\sigma_0^2}\right) \tag{3.11}$$

$$b_i = \mathrm{Im}\left|\left(z_{wi+1}-z_{wi}\right)\left(U_\infty - iV_\infty\right)\right| - \frac{1}{4\pi}\sum_{k=1}^{N_v}\Gamma_k \ln\left(\frac{\left|z_{wi+1}-z_{kj}\right|^2+\sigma^2}{\left|z_{wi}-z_{kj}\right|^2+\sigma^2}\right) - \left(V_B\cdot\hat{n}\right)\cdot\Delta s \tag{3.12}$$

The coefficients of matrix $[A]$ depend only on the geometry of the solid and the coordinates of the points where the vortices are created and their initial size. The vector $\{B\}$ is a function of the velocity of the freestream, the coordinates of the vortices in the wake and the velocity of the body. All these variables must be recalculated in each step of time.

Regardless of whether the cylinder is moving, the induced velocity of all vortex in the wake at each step of time can be calculated according to the following equations:

$$\left(u_\theta\right)_i = U_\infty - \sum_{j=1}^{n_v}\Gamma_j \frac{y_i - y_j}{2\pi\left(\left(x_i-x_j\right)^2-\left(y_i-y_j\right)^2+\sigma_j^2\right)} \tag{3.13}$$

$$(v_\theta)_i = V_\infty + \sum_{j=1}^{n_v} \Gamma_j \frac{x_i - x_j}{2\pi\left((x_i - x_j)^2 - (y_i - y_j)^2 + \sigma_j^2\right)} \tag{3.14}$$

where $(u_\theta)_i$ and $(v_\theta)_i$ are the velocity components in panel i in the x- and y- directions respectively.

New vortices are created in each step of time and it is necessary to maintain a high number of panels for the discretization in order to obtain very accurate outcomes. With this, the number of vortices increases vertiginously, which makes it impossible for longer simulations. To avoid this situation, the vortex merging technique in the wake is used, which consists in merging pairs of vortices into single vortices that satisfy certain conditions. Accordingly, [9], one of these conditions is the following:

$$\frac{|\Gamma_1 \Gamma_2|}{|\Gamma_1 + \Gamma_2|} \frac{|z_1 - z_2|^2}{(D_0 + d_1)^{1,5} (D_0 + d_2)^{1,5}} < V_0 \tag{3.15}$$

where d_1 and d_2 are respectively the distances of the z_1 and z_2 coordinates of the old vortices to the nearest point of the body wall, and D_0 is a control parameter of the density of the vortices in the wake. The Eq. (3.15) has velocity dimension. V_0, which is a merging parameter, has a value of the order of $10^{-4} U_\infty$ and doesn't have to be a constant and can be regulated to conserve the number of vortices. The positions and velocity circulations of the new vortex elements can be given as follows:

$$\Gamma = \Gamma_1 + \Gamma_2 \tag{3.16}$$

$$Z = \frac{\Gamma_1 z_1 + \Gamma_2 z_2}{\Gamma} \tag{3.17}$$

Eq. (3.16) and Eq. (3.17) make sense, in this approach the vortices are seen as a system of particles and certain properties as a system of particles are fulfilled. Therefore, the resulting vortex circulation is the sum of the circulations of the old vortices, related to the sum of the masses in the particle system, and the position of the new vortex is a linear combination of the positions of the old vortices, similar to the calculation of the mass center in System of particles.

[10] recommends having a higher concentration of vortices in the wall of the body and that vortices of low circulation are associated with some of greater circulation. Thus, the concentration of the vortices is dense near the body and gradually disperses as they move away. Therefore, one of the criteria for merging of vortices involves that they are quite separate from the body.

Another criterion was given by [5], the merging between vortices is strictly done in pairs, that is, between the vortices of the same signal. Those who have undergone the merging mechanism are prohibited from performing the process again.

MDV, proposed by [9], is used in the work that satisfies the following conditions:

1. Initial conditions for the entire domain including the boundary (at t = 0):

$$\text{Irrotationality:} \quad \omega = 0 \tag{3.18}$$

$$\text{Circulation equal to zero:} \quad \Gamma = \int \omega \cdot \hat{n} dA = 0 \tag{3.19}$$

2. Boundary conditions:

$$\text{on body: } u \cdot \hat{n} = V_B \cdot \hat{n} \tag{3.20}$$
$$\text{far: } u \to U_\infty \quad \text{where} \quad |r| \to \infty \tag{3.21}$$

[10] reports that the MVD presented by [9] was based on the potential theory and, in this case, the normal velocity condition on the wall of the body, Eq. (3.9), is sufficient. Nevertheless, in the simulation of the flow must take into account the non-slip condition, i.e., the relative tangential velocity between the surface of the body and the flow is zero. For this σ_0, which appears in the Eq. (3.11), should be determined according to $\sigma_0 = \dfrac{\Delta s}{2\pi}$, to ensure that the induced velocity by this same vortex is zero on the wall and thus satisfy this condition. To calculate the hydrodynamic forces, we need to calculate the pressure in each panel:

$$p_i = p_0 - \rho \frac{\Delta \Gamma_i}{\Delta t} \tag{3.22}$$

where p_0 is a reference pressure and can be regarded as zero and Γ_i is the circulation created in panel i minus the circulation absorbed by panel i. The force in the panel i is calculated numerically as follows:

$$F = -\sum_{i=1}^{N_w} p_i \Delta s_i \hat{n} \tag{3.23}$$

Reducing the hydrodynamic force, Eq. (3.23), in terms of the fluid density ρ, the velocity of the freestream U_∞ and the diameter of the cylinder D, one can determine the drag and lift coefficients defined as:

$$C_D = \frac{F \cdot \hat{n}_x}{\frac{1}{2}\rho U_\infty^2 D} \tag{3.24}$$

$$C_L = \frac{F \cdot \hat{n}_y}{\frac{1}{2}\rho U_\infty^2 D} \tag{3.25}$$

4 Results

We present the results using the computational tool developed in this work to simulate the cases of vertical risers subjected to a uniform velocity profiles. The ends of the riser are free to rotate but not to translate. The mass, damping and stiffness matrices were constructed using the parameters of a real riser proposed by [4], which are given in Table 1.

Table 1: Parameters of a real riser.

Parameter	**Value**
Outer diameter (m)	0,25
Internal diameter (m)	0,21106
Elastic modulus (Pa)	$2,1 \times 10^{11}$
Density of external fluid (kg/m^3)	1025
Density of internal fluid (kg/m^3)	800
Density of structural material (kg/m^3)	7700
Depth of water line (m)	100
Length (m)	120
Axial force on top - roughly 1,5 times the proper weight (kN)	200

The riser was modeled with 50 finite elements of the same length below the water line and 10 elements above the water line. Previous simulations were performed to identify the dominant modes which depend on the velocity of the marine current. Two dominant modes were used with a damping factor (ζ) equal to 2% for each mode. The simulated velocities and their corresponding Reynolds numbers are shown in Table 2.

Table 2: Marine current velocities and their corresponding Reynolds numbers.

U_∞(m/s)	Re
0,2334	$5,83 \times 10^4$
0,3890	$9,72 \times 10^4$
0,6223	$1,56 \times 10^5$
0,8557	$2,14 \times 10^5$

Figure 3 shows the envelope of the riser in the xz plane for a current velocity $U_\infty = 0,2334$ m/s. The line of envelope closest to the riser axis is a static equilibrium configuration of the riser when it is subjected to the drag of marine current and which was previously calculated. Also, Figure 3 shows the envelope of the displacements in the plane yz also for $U_\infty = 0,2334$ m/s, where it is observed that the riser is in its first mode shape. In Figure 3 also the displacements obtained by [10] were superimposed, observing a consistency of results.

Figure 4 shows, for the velocity $U_\infty = 0,2334$ m/s, the history of the distribution of the drag coefficient along the riser and over a dimensionless time. On the right side of the figure the values of the drag coefficient appear. It is observed that the maximum values (in red color) of the drag coefficient are in the central region of the riser. Also, Figure 4 shows the lift coefficient distribution over dimensionless time. It is also observed that in the central region of the riser the highest lift forces are developed. These results for the distribution of drag and lift coefficients are consistent with the movement of the structure that presents the highest velocity in its central region and, therefore, higher hydrodynamic forces.

In the case of current velocity m/s, Figure 5 and Figure 6 present results with the same tendency as the results obtained in the case of current velocity $U_\infty = 0,3890$ m/s. The riser immersed in a marine current with velocity m/s has its movement dominated by the second mode shape.

Figure 7 to Figure 10 shows the results obtained for higher velocities of marine current. It is observed that by increasing the velocity, the structure oscillates in its higher natural mode shape. In addition, regions subjected to higher drag and lift forces are always located where the structure has higher velocities.

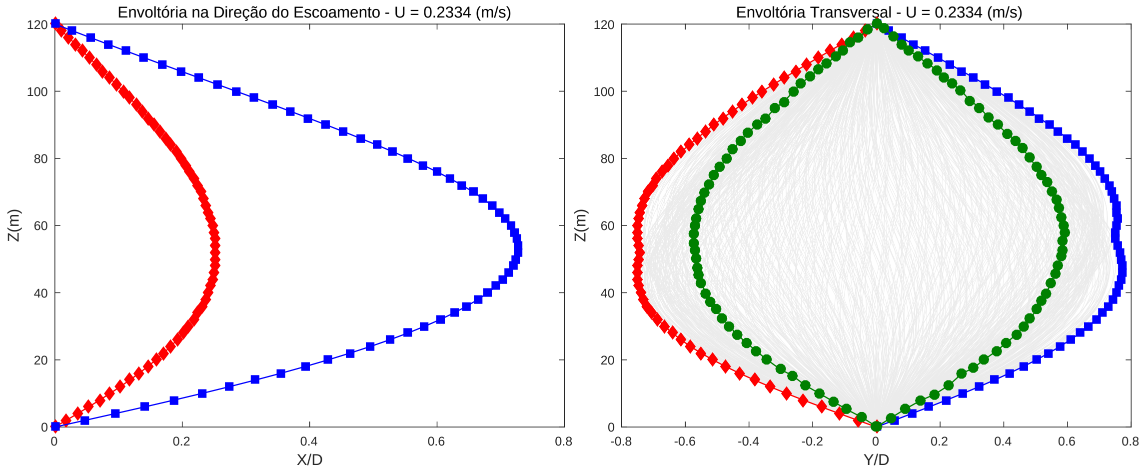

Figure 3: (Left side) In-line envelope for $U_\infty = 0,2334$ m/s with minimum displacement (in red color) and maximum displacement (in blue). (Right side) Transverse envelope for $U_\infty = 0,2334$ m/s in 2nd mode shape with minimum displacement (in red), maximum displacement (in blue) and overlapping curve presented (dark green) by [10].

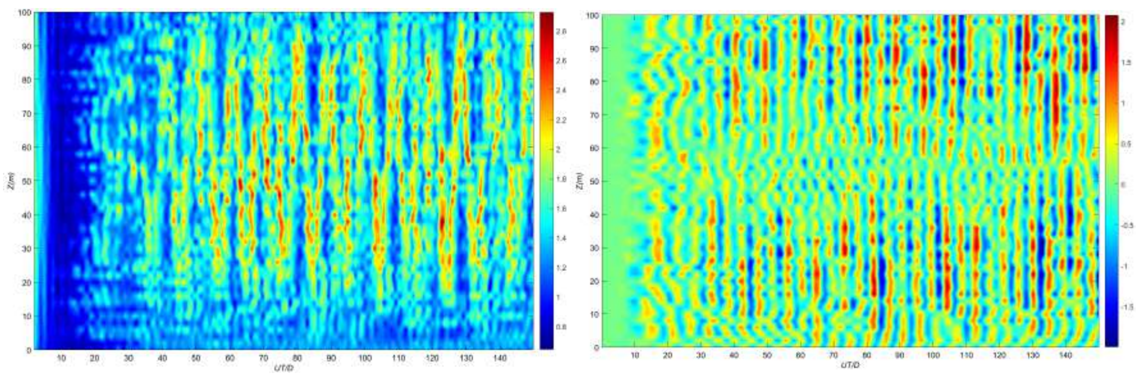

Figure 4: (Left side) Space - dimensionless time graph of the vertical riser drag coefficient subject to a uniform velocity profile $U_\infty = 0,2334$ m/s. (Right side) Space - dimensionless time graph of the vertical riser lift coefficient subject to a uniform velocity profile $U_\infty = 0,2334$ m/s.

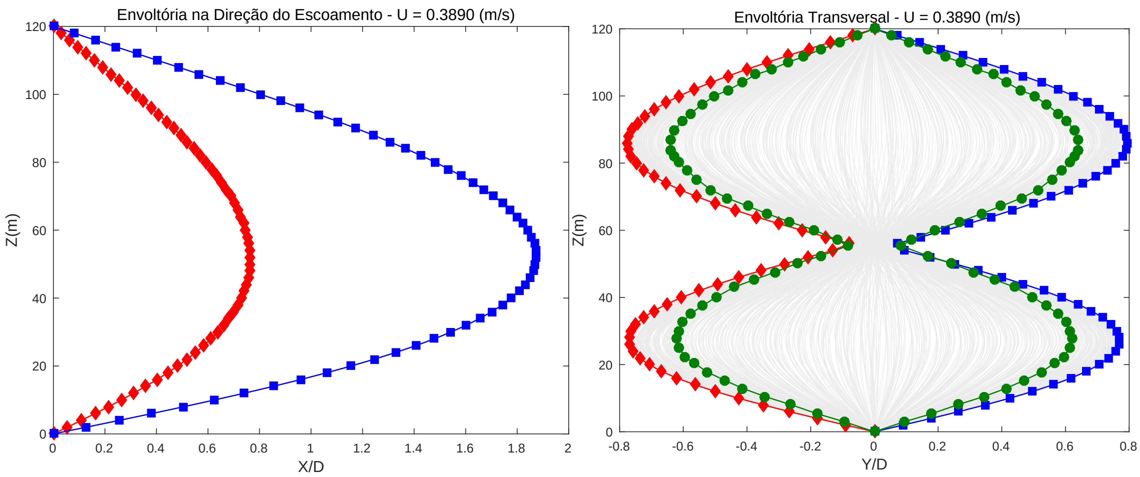

Figure 5: (Left side) In-line envelope for $U_\infty = 0,3890$ m/s with minimum displacement (in red color) and maximum displacement (in blue). (Right side) Transverse envelope for $U_\infty = 0,3890$ m/s in 2nd mode shape with minimum displacement (in red), maximum displacement (in blue) and overlapping curve presented (dark green) by [10].

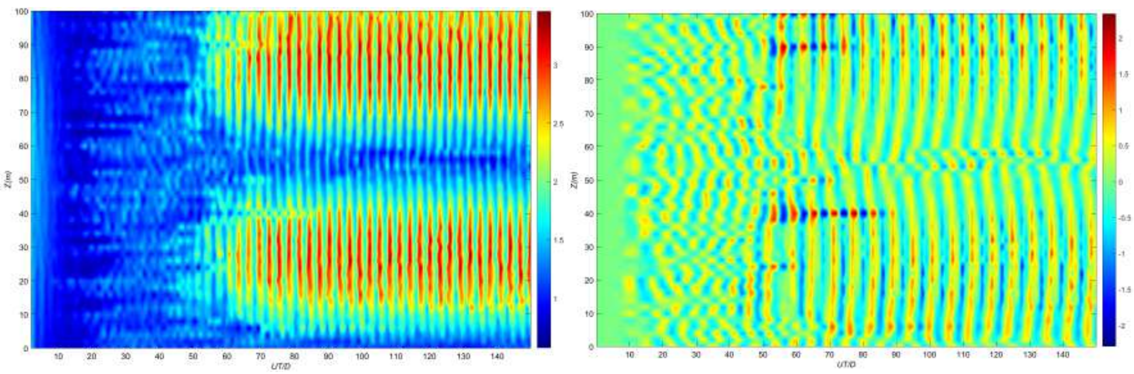

Figure 6: (Left side) Space - dimensionless time graph of the vertical riser drag coefficient subject to a uniform velocity profile $U_\infty = 0,3890$ m/s. (Right side) Space - dimensionless time graph of the vertical riser lift coefficient subject to a uniform velocity profile $U_\infty = 0,3890$ m/s.

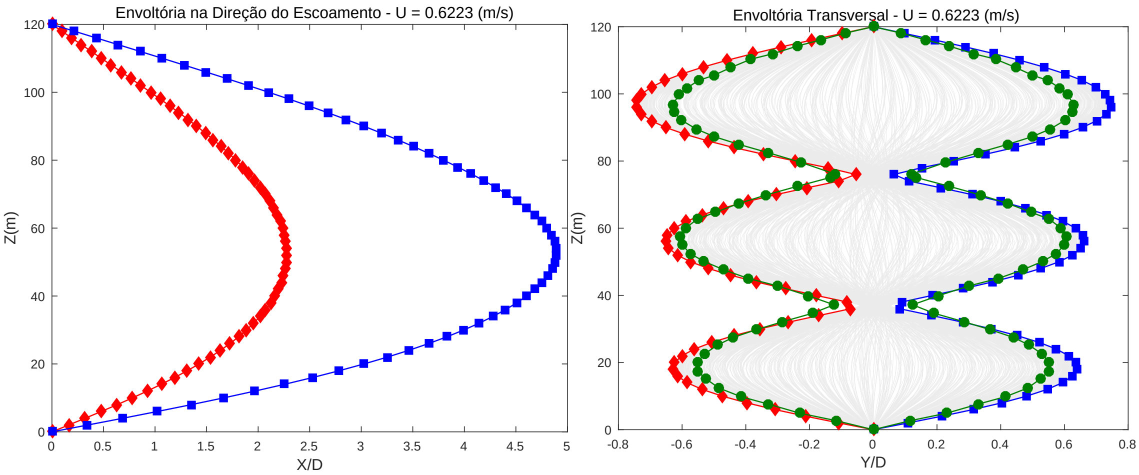

Figure 7: (Left side) In-line envelope for $U_\infty = 0,6223$ m/s with minimum displacement (in red color) and maximum displacement (in blue). (Right side) Transverse envelope for $U_\infty = 0,6223$ m/s in 2nd mode shape with minimum displacement (in red), maximum displacement (in blue) and overlapping curve presented (dark green) by [10].

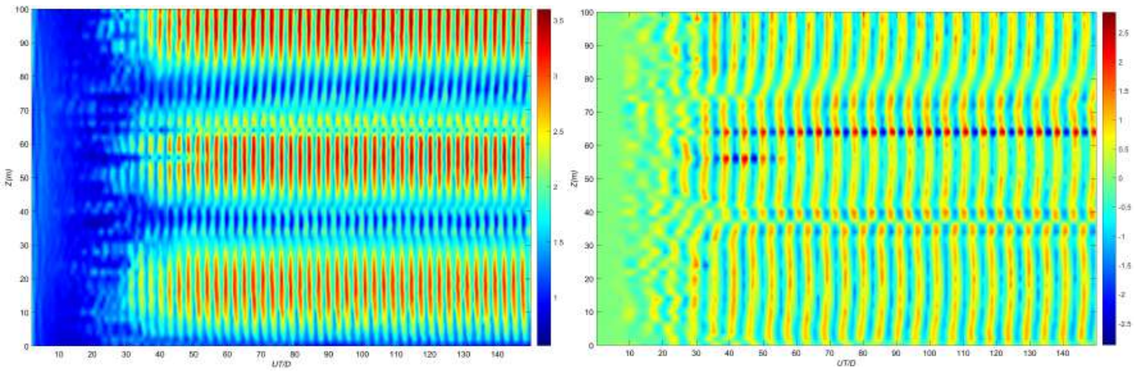

Figure 8: (Left side) Space - dimensionless time graph of the vertical riser drag coefficient subject to a uniform velocity profile $U_\infty = 0,6223$ m/s. (Right side) Space - dimensionless time graph of the vertical riser lift coefficient subject to a uniform velocity profile $U_\infty = 0,6223$ m/s.

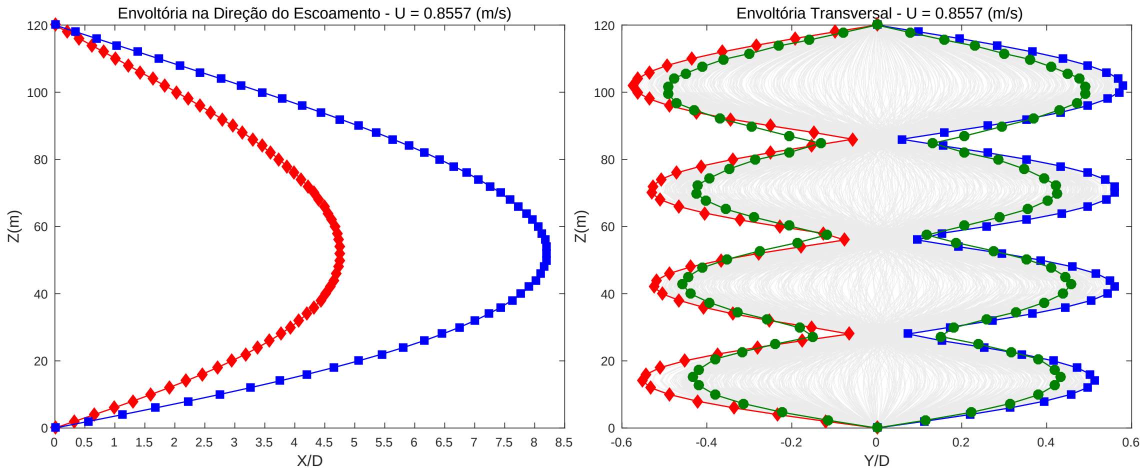

Figure 9: (Left side) In-line envelope for $U_\infty = 0,8557$ m/s with minimum displacement (in red color) and maximum displacement (in blue). (Right side) Transverse envelope for $U_\infty = 0,8557$ m/s in 2nd mode shape with minimum displacement (in red), maximum displacement (in blue) and overlapping curve presented (dark green) by [10].

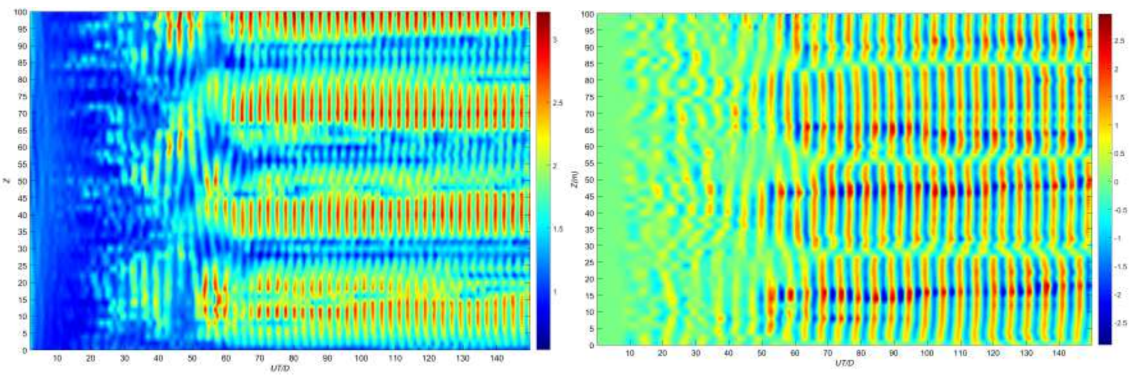

Figure 10: (Left side) Space - dimensionless time graph of the vertical riser drag coefficient subject to a uniform velocity profile $U_\infty = 0,8557$ m/s. (Right side) Space - dimensionless time graph of the vertical riser lift coefficient subject to a uniform velocity profile $U_\infty = 0,8557$ m/s.

5 Discussions

The computational tool still in development presents different results than expected, in relation to the numerical results presented by [10]. The causes can be due to the implementation of the DVM, the elastic base equation or the use of the explicit method. In addition, for [10] a possible reason for the discrepancy between the numerical results and the experimental results is to assume a two-dimensional flow. Although, [10] indicates that such a reason is only reasonable in view of the fact that large vibration amplitudes seem to eliminate the three-dimensional ones observed in the wake [2].

6 Conclusions

This work presents limitations in both the structural and hydrodynamic model. The first is limited to small displacements and the last partially simulates the effects of viscosity. They are justified by the need for efficient computational tools for its day-to-day use in deep-water riser analysis and design. The research line focuses on developing efficient computational tools, using improved or corrected methods that can study real and practical problems. The future researches in the structural model suggest to look for other ways of building the damping matrix, which involve not only the dominant vibrating modes, but all modes of vibration and develop a model that involves the cases of risers arranged in catenary. In the hydrodynamic model suggest to develop works as: using the most recent convection methods, the Fast Multipole Method is used, which uses an auxiliary mesh to calculate the induced velocities by groups of vortices, reducing the number of operations to $O(N)$ or $O(N \log N)$ and consider the effects of the boundary layer in hydrodynamic model.

References

[1] P. W. Bearman, Circular cylinder wakes and vortex-induced vibrations, Journal of Fluids and Structures, Vol. 27, pp. 648-658, (2011), DOI: 10.1016/j.jfluidstructs.2011.03.021.

[2] R. D Blevins, Flow Induced Vibration, Krieger Publishing Company Co., Florida, 2nd edition, (1990).

[3] C. S. Desai and J. F. Abel, Introduction to the Finite Element Method, Journal of Fluid Mechanics, Vol. 58, Issue 1, pp. 206-207, (1973), DOI: 10.1017/S0022112073212247.

[4] J. A. Ferrari, Hydrodynamics Loading and Response of Offshore Risers, Ph.D thesis, Imperial College London, (1998).

[5] R. B. Flatschart, Simulação numérica paralela do escoamento ao redor de risers, Tese de Doutorado, USP, (2007).

[6] M. H Patel. and J. A. Witz, Compliant Offshore Structures, Butterworths-Heinemann, Oxford, 1st edition, (1991).

[7] T. Sarpkaya, A critical review of the intrinsic nature of vortex-induced vibrations, Journal of Fluids and Structures, Vol. 19, pp. 389-447, (2004), DOI: 10.1016/j.jfluidstructs.2004.02.005.

[8] E. A. Santos, Vibração Induzida por Vórtices em Cilindros com Alta Razão de Aspecto: Simulações Numéricas e Comparações com Resultados Experimentais, Tese de Doutorado, USP, (2011).

[9] P. R. Spalart, A. Leonard and D. Baganoff, Numerical Simulation of Separated Flows, Ph.D thesis, Standford University, (1983).

[10] C. T. Yamamoto, Estudo do escoamento tridimensional ao redor de un agrupamento de cilindros lado a lado, Dissertação de Mestrado em Engenharia Naval e Oceânica, USP, (2002).